

# Application of cellular automata method to simulate the hot deformation behavior of a dual phase titanium alloy

R. Bastajib, N. Boutana, P. Bocher, M. Jahazi

*A mathematical model based on the Eshelby theory and using the cellular automata method (CA) is developed to study microstructure evolution during forging of two-phase alloys. Specifically, the method is applied to the case of near alpha titanium alloy, IMI834, mainly used in the high-pressure parts of axial compressors of the most recent gas turbine engines. Viscoplastic laws are used to describe the flow behavior of this alloy for equiaxed microstructures. The results obtained by CA models can reasonably well describe the material behavior both in the high temperature beta phase and in the two phase alpha + beta region. Experimental data of hot compression in the pure beta field are exploited in order to quantify the thermomechanical behavior of this phase, then processing in the alpha + beta field are used to calculate  $\alpha$  phase behavior. Comparisons between the numerical modelling results and the experimental ones indicates that the CA method has a good capability for predicting the influence of forging conditions on the local and global mechanical characteristics of IMI834 alloy.*

## 1. Introduction

In titanium alloys, local microstructural changes (Germain et al. 2005) can generate damage in service with disastrous consequences (Bach and Evans 1983; Toubal et al. 2009; Uta 2009). This problem becomes of paramount importance when it comes to Ti alloys used for aerospace applications and results in premature removal of parts from service as a precautionary measure. It was shown that these heterogeneities are generated during deformation (Germain 2007) and that proper thermomechanical processing can reduce or even cancel their detrimental effects (Uta 2009).

The large number of the process parameters that could contribute to control the generation and obliteration of these texture heterogeneities, justify a better understanding of the relationship between the micro and macro behavior of titanium alloys during processing. In recent years with the advent of powerful numerical methods it has become possible to simulate multivariable manufacturing processes and predict the behavior of the component. The finite element method, self consistent models (Semiatin et al. 2002) and recently the cellular automata method (CA) (Boutana et al. 2008) are the major numerical methods used to carry out the above mentioned studies. All three methods allow to study both local and global behavior of the material, an advantage that is absent in all experimental methods. Among these methods, the CA method has the great advantage of being more flexible with much shorter calculation times (Boutana et al. 2008).

In the present work, a computer code using the CA method based on Eshelby's (1957) approach is developed to study the mechanical behavior of a heterogeneous two phase material. The flow behavior prediction is applied to the hot deformation of a near-alpha titanium alloy and the effect of phase proportion and phase morphology is studied. The selected alloy is the IMI 834 which is used in the compressor section of aircraft engines. The forging routes for such parts require severe deformations in the two-phase field to attain the targeted microstructure and mechanical properties.

The objectives of the present paper are then threefold:

- to develop a mathematical model using the cellular automata method based on Eshelby's mechanism to simulate the forging process of IMI 834 with equiaxed microstructure;
- to generate the nonlinear viscoplastic parameters of the IMI 834 alloy;
- to apply the CA method to study the influence of processing conditions at the local level and its impact on producing microstructural heterogeneities during the forging process.

## 2. Description of mathematical model

### 2.1. Cellular automaton approach

Cellular Automata are dynamical systems of cells whose behaviors are defined by local relations (Wolfram (1984)). Schematically, CA can be presented as a periodic space grid constructed and run in accordance with the following steps:

- Cells and their related characteristics (states) are defined.
- Relationships between neighbors are defined. In the present model a 2D hexagonal array is generated and it is assumed that each cell can only communicate with its first six neighbors.
- In order to represent schematically a microstructure, each cell is associated on a one-to-one basis with a grain, subgrain or homogeneous phase domain and its respective physical properties.
- Cell transition rules governing the evolution of the cell from one state to another are specified.
- As the CA is a timed system evolution rules are to be defined: In the present work the state of all cells change simultaneously according to the transition rule (Wolfram (1984) and Smith (1994)).

### 2.2. Generation of the initial microstructure

The generation of microstructure in CA permits the derivation of results for various topologies. The cells pertaining to each phase can be randomly distributed, aligned or packed in clusters and these clusters can also be randomly distributed or arranged according to a specific order (Briottet and Montheillet 2005). In the present work, aggregate of grains made of two distinct phases, namely  $\alpha$  and  $\beta$  are randomly generated.

Each grain is associated with a cell of two-dimensional cellular automata. The number of neighbors to each cell is assumed to remain constant and equal to six. The nearest neighbor relations are displayed in the form of the hexagonal array.

### 2.3. Application of the Eshelby theory in CA

Most of models that can give an estimate of the mechanical behavior of multiphase materials at the local level are based on Eshelby's theory. Eshelby (1957) studied an isotropic ellipsoidal inclusion with the elastic constant different from those of the isotropic infinite matrix, subject to a homogeneous deformation at infinite  $\varepsilon^\infty$  (Figure 1). His approach consists of determining the tensor of deformation in the inclusion by submitting a homogeneous medium to specific deformations (eigenstrains) without knowing the velocity field in the matrix. The specific deformations are usually non-elastic deformations.

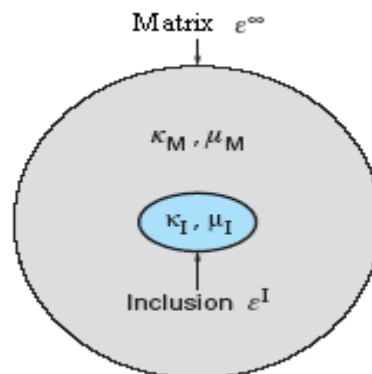


Figure 1. Schematic representation of Eshelby approach

Initially the approach of Eshelby was related to elastic materials, but was later generalised to nonlinear viscoplastic components (Montheillet and Gilormini 1996). By considering the case of uniaxial compression, the

local strain rate  $\dot{\varepsilon}^I$  applied to the inclusion I and resulting from the remote strain rate  $\dot{\varepsilon}^\infty$  at the infinite can be written as

$$\dot{\varepsilon}^I = \delta_I \dot{\varepsilon}^\infty \quad (1)$$

where  $\delta_I$  is the strain rate localization factor. The local strain rate  $\dot{\varepsilon}_{ij}^c$  of a given cell C (identified by the  $i, j$  indices in the array) is calculated in the present model using the following equation

$$\dot{\varepsilon}_{ij}^c = \frac{\delta_c}{\langle \delta_c \rangle} \dot{\varepsilon}^\infty \quad (2)$$

where  $\delta_c$  is the strain rate localization factor in the cell and  $\langle \delta_c \rangle$  the average strain rate localization factor in the entire array. For an equiaxed inclusion, the strain rate localization factor can be calculated using the following equation

$$\delta_c = \frac{(1+a)\{1 - \tanh[(b+c)(\Sigma_c - 1)]\}}{1+a+(d-1)\tanh[(b+e)(\Sigma_c - 1)]} \quad (3)$$

$a, b, c, d$  and  $e$  vary with the strain rate sensitivity coefficient  $m$  (Briottet and Montheillet 2005). As in the present case both phases have  $m$  values close to 0.2, the coefficients will be 0.69, 0.1, 0.863, 7.67 and -0.007, respectively.  $\Sigma_c$  is the consistency ratio defined by the following equation

$$\Sigma_c = \frac{k_c}{k_v} \quad (4)$$

where  $k_c$  is the viscosity of the cell and  $k_v$  is the average viscosity of the neighbors of the involved cell. The parameter  $k_v$  is given by the following equation

$$k_v = k_\alpha \left[ \left( \frac{1}{6} \right) (3 - 2\rho + 5(1 - f_{v\alpha})(\rho - 1)) + \sqrt{(3 - 2\rho + 5(1 - f_{v\alpha})(\rho - 1))^2 + 24\rho} \right] \quad (5)$$

where  $f_{v\alpha}$  is the volume fraction of the  $\alpha$  phase in the neighborhood (6 neighbors surrounding the cell), and  $\rho$  is the viscosity ratio between  $\alpha$  phase and  $\beta$  phase ( $k_\beta / k_\alpha$ ). It is important to mention that in the present work, the average strain rate localization factors  $\langle \delta_c \rangle$  is calculated by the mixture law.

After calculating the local strain rate for each cell, the local stress  $\sigma_c$  is derived from the nonlinear viscoplastic law of each phase using the following equation (Oikawa et al. 1994)

$$\sigma_p = (K_p \exp(Q/RT) \dot{\varepsilon})^{m_p} \quad (6)$$

where  $p$  represents the phase ( $\alpha$  or  $\beta$ ),  $K_p$  is a constant related to the chemical composition of the phase,  $R$  is the constant of the perfect gas,  $Q_p$  is the activation energy of the phase,  $T$  is the deformation temperature in Kelvin, and  $m_p$  is the strain rate sensitivity of the phase.

### 3. Calculation of the volume fraction of $\alpha$ and $\beta$ phases for IMI 834

The viscoplastic parameters of the phases  $\alpha$  and  $\beta$  are obtained from compression tests which have been made in pure  $\beta$  and in  $\alpha + \beta$  domains. The as-received microstructure of the specimen is composed of 20% of equiaxed  $\alpha$  phase within a transformed  $\beta$  matrix (lamellar  $\alpha$  phase) (Figure 2).

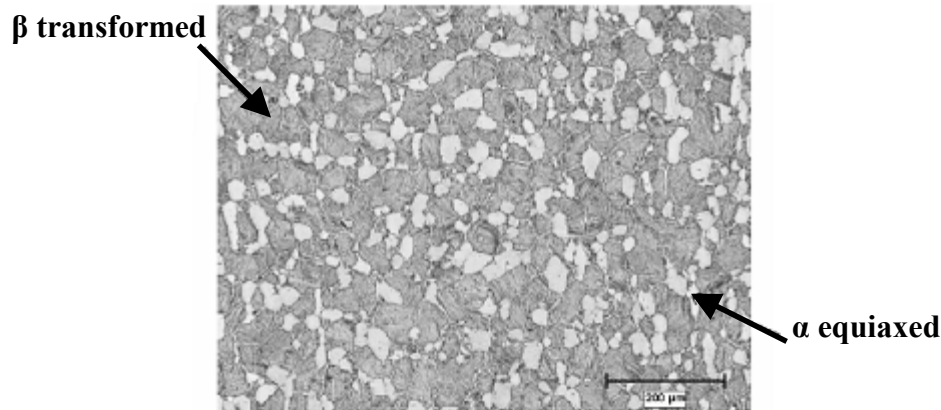


Figure 2. As-received microstructure with 20% equiaxed primary  $\alpha$  in a transformed  $\beta$  matrix

The compression tests are conducted at temperatures of 950 °C to 1100 °C, with strain rates of 0.1 s<sup>-1</sup> and 1 s<sup>-1</sup>. Deformations are ranging from 0.7 to 1.4. The samples chosen are cylindrically shaped 76 mm in diameter and 11.4 mm in length. The chemical composition of the samples used in this study is given in Table 1.

Table 1. Chemical composition of titanium alloy IMI 834

Element	Al	Sn	Zr	Nb	Mo	Si	C	Ti
Content (%)	5.8	4	3.5	0.7	0.5	0.3	0.06	balance

All samples are heated at the deformation temperature ( $T_{def}$ ) for 15 min, and deformed. Schematics of the thermal cycles for the tests are shown in Figure 3. Typical stress-strain curves, corrected for friction and adiabatic heating, display an initial work hardening period to peak stress at strains less than 0.2 followed by varied levels of flow softening (Figure 4). Steady state stress was reached rapidly at high temperatures and is approximately 15 % lower than peak values at 1060°C and above. Greater degrees of flow softening are observed at lower temperatures with the amount of softening increasing with decreasing temperature (i.e. a stress drop of ~30% at 975°C) (Figure 4).

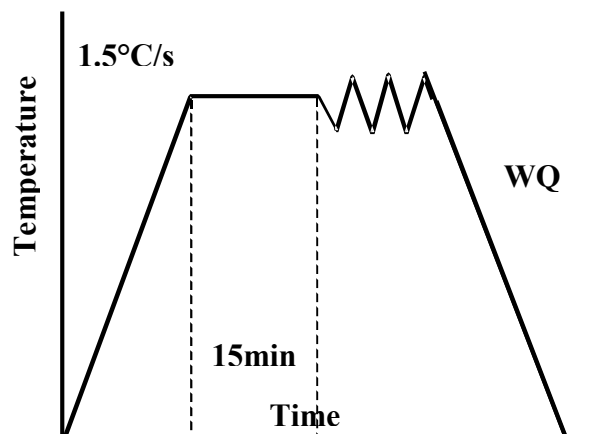


Figure 3. Schematic of heating cycle employed for an initial equiaxed

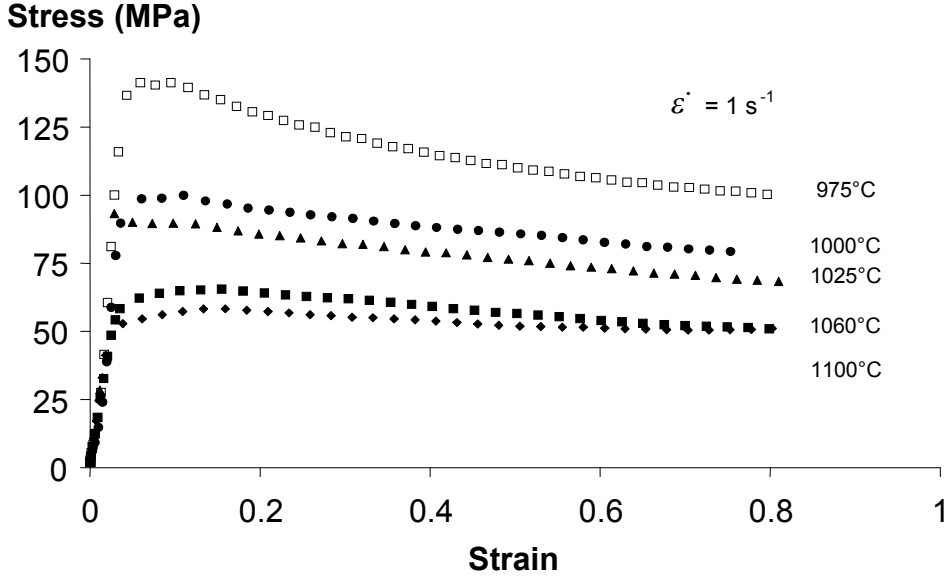


Figure 4. Stress-strain curves at a strain rate of  $1 \text{ s}^{-1}$

#### 4. Thermomechanical characterisation of each phase

##### 4.1. Steady state behavior of $\beta$ phase during hot deformation

The calculation of the local stress in the  $\beta$  phase,  $\sigma_{\beta}$  is derived from the nonlinear viscoplastic law using Equation. (6) (Oikawa et al. 1994). The description of the parameter  $K_{\beta}$  has been introduced by Semiatin et al. (2002) using published experimental curves for several titanium alloys. The authors found that the  $K_{\beta}$  parameter depends on the equivalent content of Vanadium ( $V_{eq}$ ) in the  $\beta$  phase. Thus,  $K_{\beta}$  is given by the following equation

$$K_{\beta} = 10^{(a \cdot \ln(V_{eq}) + b)} \quad (7)$$

where  $a = 1.4712$  and  $b = -1.7691$

$$V_{eq} = 0.27 Al_{eq\beta} + 0.5Sn + 2Mo + 0.3Zr + Cr + 0.4Nb + 13Si \quad (8)$$

$Al_{eq\beta}$  is the percentage of equivalent aluminum for  $\beta$  phase, and  $V_{eq}$  is the percentage of equivalent vanadium. In the dual phase region,  $Al_{eq\beta}$  changes as a function of temperature as following Vo et al. (2002)

$$Al_{eq\beta} = 0.85 \left[ (T - 45)^2 \cdot (-2.92 \cdot 10^{-5}) + 6.44 \cdot 10^{-2} \cdot (T - 45) - 29 \right] \quad (9)$$

Table 2 shows the values of  $K_{\beta}$  for different forging temperatures including the two phase region.

Table 2. Calculation of  $K_{\beta}$  values according to temperature

T (°C)	1100	1060	1025	1000	975
$K_{\beta}$	37.27	37.27	36.47	35.79	35.10

The calculation of  $Q_\beta$  and  $m_\beta$  are made from three experimental data using the steady state stress presented in Figure 4 and using the linear relation derived from Equation (6)

$$\frac{\ln(K_\beta) + \ln(\dot{\epsilon})}{\ln(\sigma_\beta)} = \frac{1}{m_\beta} - \frac{Q_\beta}{RT \ln(\sigma_\beta)} \quad (10)$$

Figure 5 shows the plot of Equation (10). The values have been found to be:  $Q_\beta = 153923$  J/mol and  $m_\beta = 0.23$  which are in agreement with those reported in the literature (Semiatin et al. 2002): 160000 J/mol and 0.23, respectively.

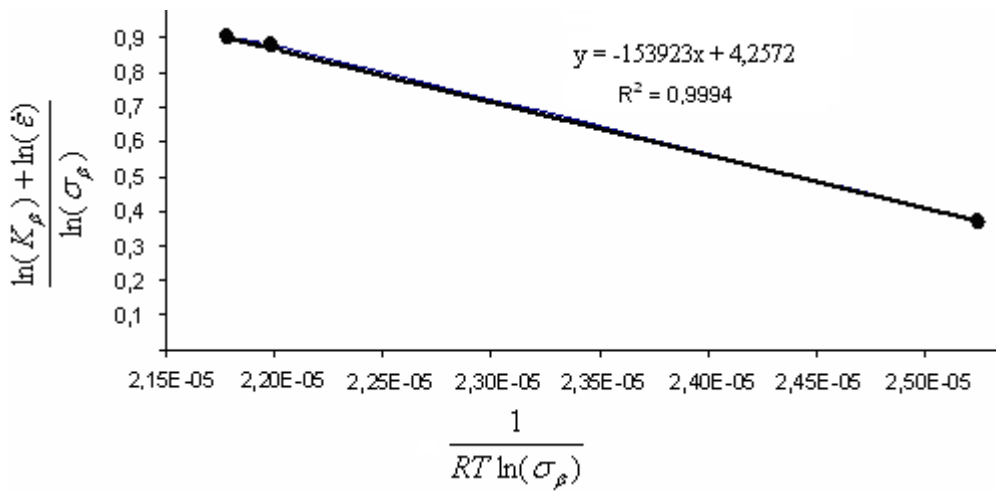


Figure 5. Graphic calculation of IMI 834 constants  $Q_\beta$  and  $m_\beta$

## 4.2. Constitutive equations for the $\alpha$ phase during steady state hot deformation

### 4.2.1. Method

The calculation of the constants governing the mechanical behavior of the  $\alpha$  phase is done in a similar manner as that of the  $\beta$  phase. The local stress of  $\alpha$  phase  $\sigma_\alpha$  is derived from the same type of nonlinear viscoplastic law (Equation 6).

The parameter  $K_\alpha$  depends on the content of equivalent Aluminum  $Al_{eq\alpha}$  from Vo et al. (2002)

$$K_\alpha = 10^{(a \cdot Al_{eq\alpha} + b)} \quad (11)$$

where  $a = 0.37$  and  $b = -3.37$

$$Al_{eq\alpha} = Al + (1/3Sn + 1/6Zr + 10C) \quad (12)$$

In contrast to  $K_\beta$ ,  $K_\alpha$  is found to be independent of the temperature and equal to 0.75 for IMI 834.

The  $\alpha$  phase steady state stress  $\sigma_\alpha$  cannot be calculated directly as there is a mixture of phases. As a first approximation,  $\sigma_\alpha$  is measured from the experimental data and applying the following law of mixture

$$\sigma_\alpha = \frac{\sigma_{\alpha+\beta} - (1 - f_\alpha)\sigma_\beta}{f_\alpha} \quad (13)$$

where  $\sigma_{\alpha+\beta}$  is the overall stress of the mixture obtained from the experimental data,  $\sigma_\beta$  is the  $\beta$  phase stress in the mixture (extrapolation in the two phases domain from results obtained in the pure  $\beta$  domain) and  $f_\alpha$  is the volume fraction of  $\alpha$  phase present during deformation.

#### 4.2.2. Measurement of the volume fraction of $\alpha$ actually present during deformation

Difficulties were met during the measurement of reel percentage of  $\alpha$  phase present during the steady state deformation. In fact, equiaxed phases (primary  $\alpha$ ,  $\alpha_p$ ) are easy to identify, some large size  $\alpha$  lamellae were present at the deformation temperature as they appear deformed when microstructures is looked at higher magnifications. This complicates the estimation of the volume fraction of the  $\alpha$  phase. Specifically, at a lower temperature ( $T_{\text{def}} = 975^\circ\text{C}$ ), microstructures look like a mixture of primary  $\alpha$  particles in a matrix of transformed  $\beta$ .

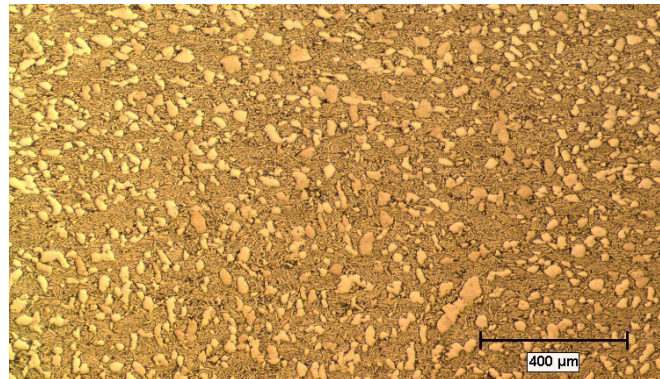


Figure 6. Equiaxed microstructure obtained after deformation at  $T_{\text{def}}=975^\circ\text{C}$ ,  $\dot{\epsilon}=0.1\text{s}^{-1}$ ,  $\epsilon=1$

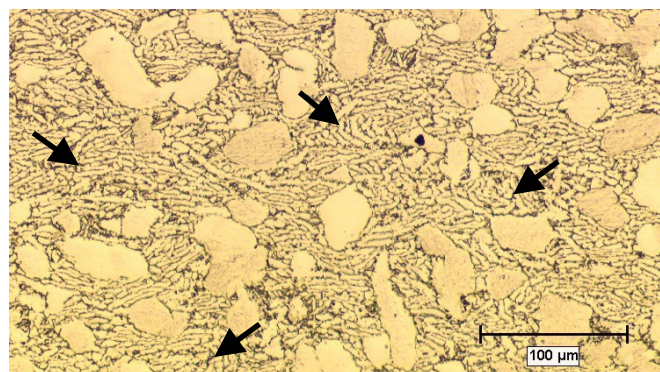


Figure 7. Equiaxed microstructure obtained after deformation at  $T_{\text{def}}=975^\circ\text{C}$ ,  $\dot{\epsilon}=0.1\text{s}^{-1}$ ,  $\epsilon=1$  (Arrows pointing out the presence of deformed coarse lamellar structures)

However, at a higher magnification large deformed lamellar  $\alpha$  can be clearly distinguished. The fact that these lamellae are deformed proves that they are present during the deformation of the alloy. Figure 8 shows a higher magnification view of a region where a mixture between equiaxed grains, lamellar  $\alpha$  phases (coarse and deformed) and light straight lamellar phases of transformed  $\beta$  are visible. The quantification of the volume fraction of these large coarse lamellar  $\alpha$  regions is particularly difficult but essential in order to accurately determine the volume fraction of  $\alpha$  phase present at the deformation temperature.

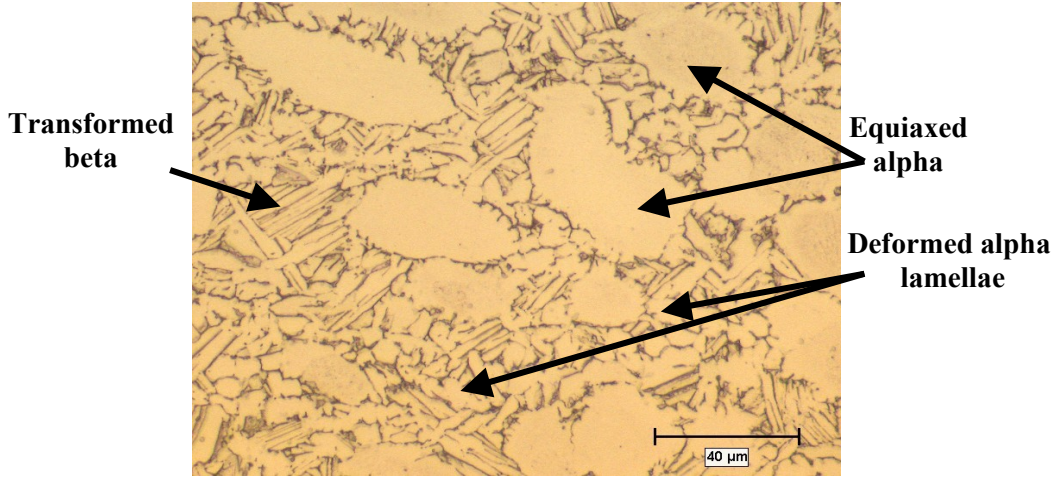


Figure 8. Microstructure deformed at  $T_{\text{def}}=975^{\circ}\text{C}$ ,  $\dot{\epsilon} = 1\text{s}^{-1}$ ,  $\epsilon = 1$  showing deformed lamellar  $\alpha$  and transformed  $\beta$  phase

The volume fraction of the deformed lamellar  $\alpha$  phase ( $f_{\alpha C}$ ) is evaluated from high magnification micrographs taken from different regions of the sample. Table 3 shows the percentages of primary equiaxed  $\alpha$  phase ( $f_{\alpha P}$ ), the percentage of the deformed lamellar  $\alpha$  phase in the rest of the microstructure  $f_{\alpha C}$  (equiaxed zone not included) and the percentage of the lamellar  $\alpha$  phase (t) present during the deformation  $f_{\alpha U}$ , in the entire microstructure for different temperatures calculated from the following equation

$$f_{\alpha U} = f_{\alpha C} \cdot (1 - f_{\alpha P}) \quad (14)$$

Using the above analysis, the total volume fraction of the  $\alpha$  phase present in the microstructure during deformation is obtained by adding the volume fraction of lamellar  $\alpha$  phases  $f_{\alpha U}$  to the volume fraction of equiaxed  $\alpha$  phase  $f_{\alpha P}$ :

$$f_{\alpha} = f_{\alpha P} + f_{\alpha U} \quad (15)$$

Table 3. Volume fractions for various temperatures

	975( $^{\circ}\text{C}$ )	1000( $^{\circ}\text{C}$ )	1025( $^{\circ}\text{C}$ )
$f_{\alpha P}$ (%)	23	20	10
$f_{\alpha C}$ (%)	46	14	6
$f_{\alpha U}$ (%)	36	10	5

As shown in Table 4, a comparison between the results obtained in this investigation and those reported in Flower (1990) indicates a relatively good agreement with those measured by Neal et al. 2001. The difference in values between the three measurements in the literature could be due to differences in the morphology of samples under investigation and the techniques used to quantify the coarse and deformed lamellar  $\alpha$  phases volume fraction  $f_{\alpha c}$ .

Table 4. Volume fractions for various temperatures found in the literature

	975( $^{\circ}C$ )	1000( $^{\circ}C$ )	1025( $^{\circ}C$ )
Flower (1990)		45	12
Neal (2001)	60	32	12
Neal (1985)	47	28	12
present work	60	30	15

#### 4.2.3. Thermomechanical processing parameters

Using Equation (13) and the volume fraction of the  $\alpha$  phase calculated above, the values of  $Q_{\alpha}$  and  $m_{\alpha}$  for IMI834 are obtained and are presented in Figure 9. These values are close to the values reported in the Semiatin et al. (2002): 273000 J/mol and 0.20, respectively.

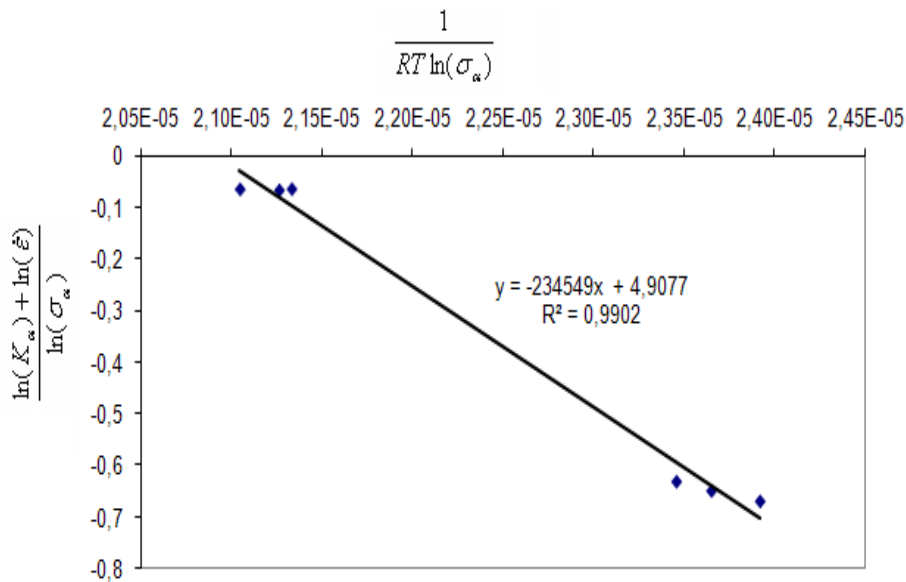


Figure 9. Calculation curve for  $Q_{\alpha}$  and  $m_{\alpha}$  for IMI 834

#### 4.3 Summary of the phase parameters

To recapitulate the calculation results, the activation energies and strain rate sensitivities of  $\alpha$  and  $\beta$  phase used for the simulations are presented in Table 5.

Table 5. Values of activation energies and strain rate sensitivities for  $\alpha$  and  $\beta$  phases

	Phase $\alpha$	Phase $\beta$
$Q$ (J/mol)	234549	153923
$m$	0.20	0.23

## 5. CA results and discussion

To show the possibilities of CA to study the local and global mechanical characteristics of a typical dual phase forging, an equiaxed microstructure consisting of  $\alpha$  phases randomly dispersed in a  $\beta$  matrix is simulated and analyzed in detail. Figure 10 shows the spatial distribution of the phases of a typical simulated microstructure (in this case, 15%  $\alpha$ ). Three local regions of interest are selected in the microstructure are illustrated in Figure 10: Zone 1, where an  $\alpha$  cell is immersed in a  $\beta$  environment, zone 2 where a  $\beta$  cell is surrounded by an  $\alpha$  environment; and finally zone 3 where the maximum stress of microstructure is located.

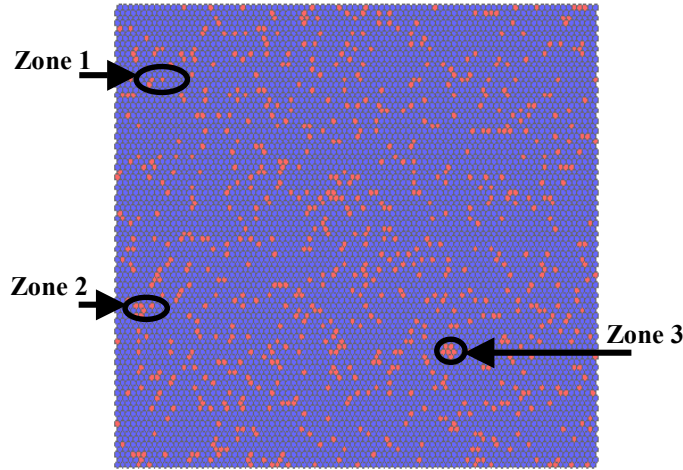


Figure 10. Microstructure studied with three zones

### 5.1. Prediction of alloy mechanical properties

From a global viewpoint, the CA model validation is made by comparing the steady state stress obtained experimentally ( $\sigma_{EXP}$ ) with those obtained by CA method ( $\sigma_{CA}$ ) and those obtained by using the law of mixture ( $\sigma_{ML}$ ) for different forging conditions of IMI 834 (Table 6).

Table 6. Comparison between the experimental results and results given by cellular automata and mixture law

T ( $^{\circ}C$ )	975	1000	1025	975	1000	1025
$\dot{\epsilon}$ ( $s^{-1}$ )	1	1	1	0.1	0.1	0.1
$\sigma_{EXP}$ (MPa)	85	76	68	54	45	40
$\sigma_{CA}$ (MPa)	86	75	68	52	44	40
(Margin of error)	1.17	-1.31	0	-3.70	0.73	0
$\sigma_{ML}$ (MPa)	86.51	79.77	86.32	52.81	48.68	40.35
(Margin of error)	0.58	6.36	0.11	-1.53	8.23	0.86

In general, the CA model results are in agreement with the experimental ones and provide good estimates for the mechanical behavior of the alloy, although they have the tendency to somewhat underestimate by few percentages the experimental data. On the other hand, the same calculations of stress values for forging conditions based on the mixture law  $\sigma_{ML}$ , overestimate the steady state flow stress.

The relatively lower flow stress values predicted by the CA method are probably due to the fact that in the CA approach, not all cells deform with the same strain rate. In fact, as indicated in the CA analysis, not all cells of a

given phase deform similarly which is logical as the strain rates in the  $\alpha$  phase are somewhat smaller than those in the  $\beta$  phase. Moreover, the behavior of the grain is a function of its neighborhoods.

## 5.2. Mechanical properties at the local level

Simulations are presented for a strain rate of  $1 \text{ s}^{-1}$  and for a case with 15 %  $\alpha$  phase. As mentioned before, the histogram in Figure 11 shows that the strain rates in the  $\alpha$  phase are globally smaller than those of the  $\beta$  phase. On the other hand, the histogram of stress values shows that the stress values in the  $\beta$  phase are smaller than those in the  $\alpha$  phase (Figure 12).

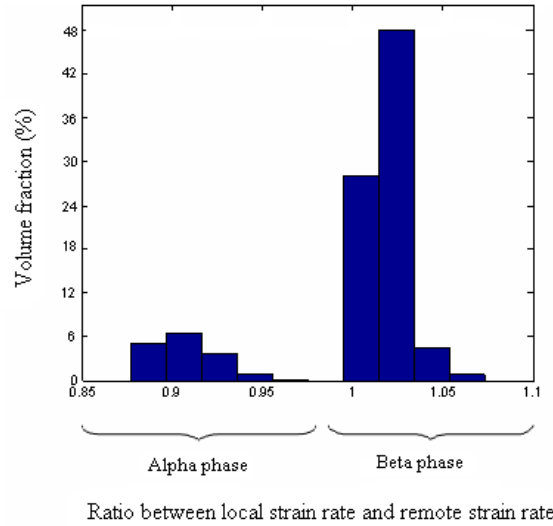


Figure 11. Histogram of strain rate distribution in the microstructure for  $\dot{\epsilon} = 1 \text{ s}^{-1}$

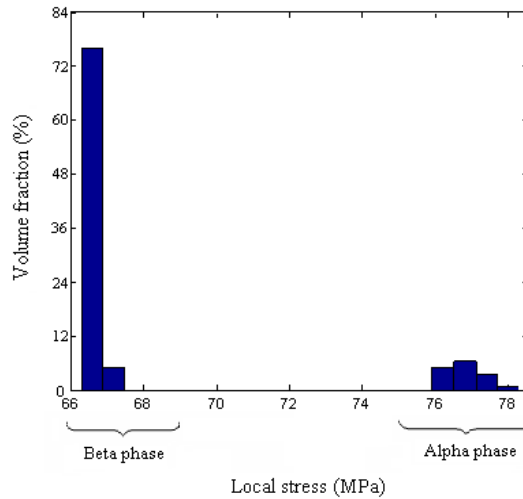


Figure 12. Histogram of stress distribution in the microstructure for  $\dot{\epsilon} = 1 \text{ s}^{-1}$

Similar results are found at local level in zone 1 (Figure 13). The local stress of the  $\alpha$  cell is higher by 14% than those of its  $\beta$  neighbors. A stress of an  $\alpha$  grain surrounded by a pure  $\beta$  environment is lower by 2% compared with  $\alpha$  grain surrounded by ( $\alpha + \beta$ ) neighborhood. On the other hand, the analysis of strain rates shows that the strain rate is minimal in the  $\alpha$  cell, while its neighborhood deforms faster than the average (about 1.66%).  $\alpha$  cells, since they have a viscosity coefficient higher than that of  $\beta$  cells, they deform less rapidly than their neighbors. This increases locally the strain rate of their  $\beta$  neighborhood.

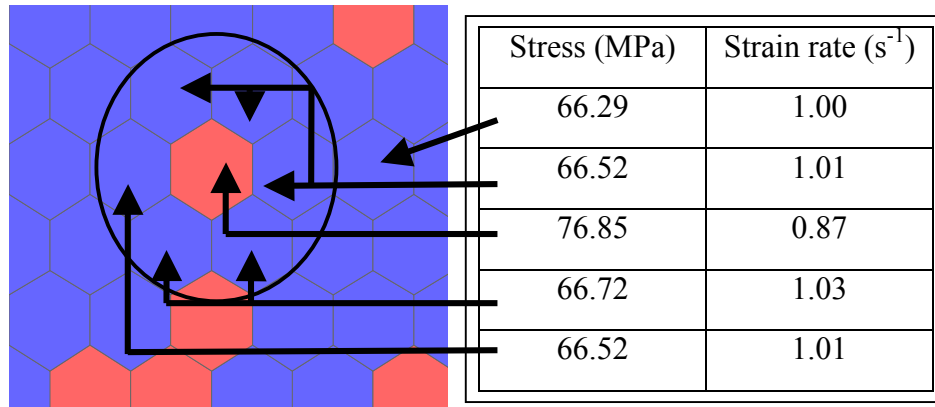


Figure 13. Zoom of zone 1 where  $\alpha$  cell is surrounded by six  $\beta$  neighbors: Representation of stress and strain rate distribution in the microstructure during forging in the steady state for  $\dot{\epsilon} = 1 \text{ s}^{-1}$

In the second zone a  $\beta$  cell surrounded by six  $\alpha$  neighbors can be seen (Figure 14). The CA analysis shows that the stress in the  $\beta$  cell increases by 1.55% compared to the global stress. It also deforms faster than its neighbors by 13%. This is due to the influence of the neighborhood ( $\alpha$  grains) which tend to transfer some pressure on the  $\beta$  cell by increasing the rigidity of the neighborhood.

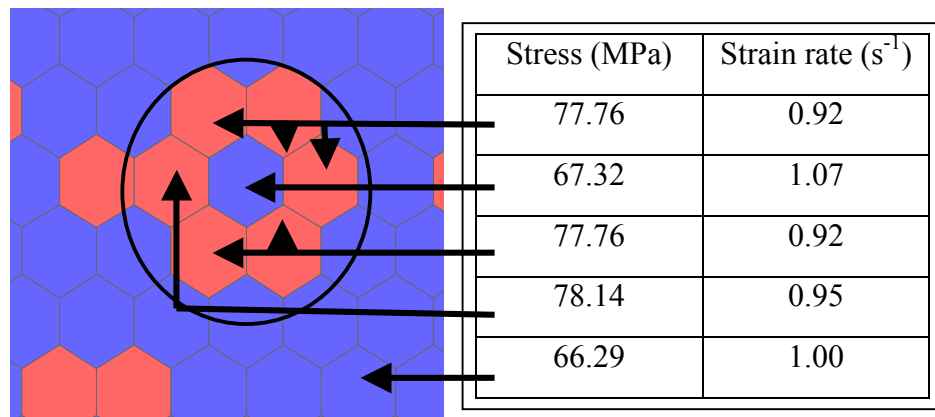


Figure 14. Zoom of zone 2 where  $\beta$  cell is surrounded by six  $\alpha$  neighbors: Representation of the distribution of stress and strain rate in the microstructure during the forging in the steady state for  $\dot{\epsilon} = 1 \text{ s}^{-1}$

Zone 3 (see Figure 15) locates the maximum stress in the microstructure. The value of the maximum stress is located in an  $\alpha$  cell whose neighborhood is made up of several  $\alpha$  cells. The stress of this cell reaches a value of 78 MPa, i.e., an increase of 2% compared with an  $\alpha$  grain imbedded in a pure  $\beta$  environment, and 12 % higher than the average steady state flow stress of 68 MPa.

In fact, the neighborhood of the  $\alpha$  grain influences the stress level that it reaches when undergoing deformation. It was noted that the greater the number of  $\alpha$  neighbors, the greater is the stress of the  $\alpha$  grain. Moreover the maximum strain rate is located on a  $\beta$  cell while the minimum stress is located in  $\beta$  grains immersed in a  $\beta$  region.

Future development taking into account the heterogeneous nature of the elastic properties of the  $\alpha$  phase will provide more comprehensive results and maybe an explanation for the occurrence of large microstructure heterogeneities in forged parts.

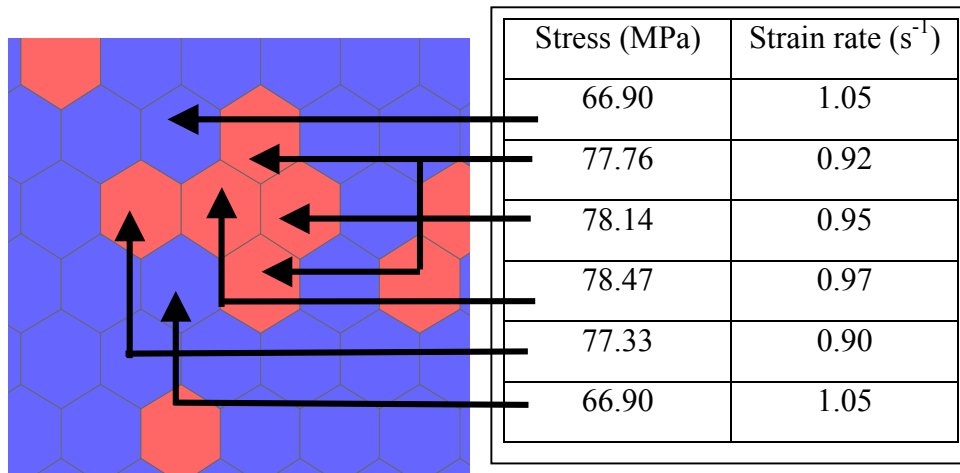


Figure 15. Expansion of zone 3 where there is maximum stress: Representation of stress distribution in the microstructure during the forging in the steady state for  $\dot{\epsilon} = 1 \text{ s}^{-1}$

## 6. CONCLUSIONS

A mathematical model using CA and based on Eshelby's inclusion is developed to better understand the processing of forged titanium alloy IMI 834 forging. The following conclusions can be drawn from this study:

- Globally the CA model results are in agreement with experimental results. Moreover, as the CA gives the opportunity to look at the local information, it is found that the local strain rates are quite close to the value of the remote strain rate with the local strain rates of  $\alpha$  grains being lower than that of the  $\beta$  matrix. On the other hand, the strain rate of the  $\beta$  phases is higher than the remote strain rate.
- It is observed that the stress of the  $\alpha$  grain is significantly higher than that of the surrounding  $\beta$  neighborhood. Within the microstructure, the maximum stress is located at the  $\alpha$  grains. It is noticed that the local stress level increases with the percentage of the  $\alpha$  grains in the neighborhood. By contrast, the stress in the  $\beta$  grains increases as the percentage of  $\alpha$  phase increases in the neighborhood.

The present work shows how CA could be used to investigate the deformation of multiphase alloys. Interesting trends have been shown, however, more features should be considered to better explain the heterogeneous deformation of bimodal near alpha titanium alloys.

## Acknowledgement

The author wishes to gratefully acknowledge the Natural Sciences and Engineering Research Council of Canada for the financial support of this work and Phoung Vo for many fruitful discussions and access to relevant data.

## References

- Bach, M.R.; Evans, W.J.: Sensitive fatigue response of titanium alloys for power plants application. *J. of Engineering for Gas Turbines and Power*, Vol. 125, (2003) 241–245
- Boutana, N.; Bocher, P.; Jahazi, M.; Piot, D.; Montheillet, F.: Microstructural modeling of cold creep/fatigue in near alpha titanium alloys using cellular Automata Method. *Transactions of the Canadian Society for Mechanical Engineer*, 32, 2, (2008), 195-223.
- Eshelby, J.D.: The determination of the elastic field of an ellipsoidal inclusion and related problems. *Proc.Roy.Soc, A* 241, (1957), 376-396.

- Germain, L.; Gey, N.; Humbert, M.; Bocher, P.; Jahazi, M.: Analysis of sharp microtexture heterogeneities in a bimodal IMI 834 billet. *Acta Materialia*, 53, 13, (2005), 3535-3543.
- Germain, L.; Vo P.; Gey N.; Jahazi M.; Humbert M.; Bocher P.: Development of sharp local alpha microtextures during alpha/beta thermo-mechanical processing of TIMETAL 834, Ti-2007 (Kyoto) Science and Technology, *Japan Institute of Metals*, 2, (2007), 925-928.
- Flower, H.M.: Microstructural development in relation to hot working of titanium alloys. *Material Science and Technology*, 6, (1990), 1082-1092.
- Smith, M.A.: Cellular Automata Methods in Mathematical Physics. Ph.D. Thesis, Massachusetts Institute of Technology, (1994), 15-45.
- Briottet L.; Montheillet F.: Prédiction des hétérogénéités de déformation dans un agrégat de deux phases viscoplastiques, *La Revue des Métallurgie-CIT/Science et génie des matériaux*, (1997), 94:1212
- Montheillet, F.; Gilormini, P.: Predicting the mechanical behavior of two phase materials with cellular automata. *Int. J. Plasticity*, 12, (1996), 561-574.
- Neal, D.F.: Materials Design Approaches and Experiences. In: J.C. Zhao; M. Fahrman; Pollock, T.M, eds., TMS, Warrendale, (2001), 199-213.
- Neal, D.F.: Titanium Science and Technology, Deutsche Gesellschaft für Metallkunde. In: G. Lütjering; U. Zwick; W. Bunk, eds., Oberursel, (1985), 2419-2424.
- Oikawa, H.: Metallurgy and technology of practical titanium alloys. In: S. Fujishiro; D. Eylon; T. Kishi, eds., TMS, Warrendale, (1994), 267-274.
- Semiatin, S. L.; Montheillet F.; Shen, G.; Jonas, J. J.: "Self-Consistent Modeling of the Flow Behavior of Wrought Alpha/Beta Titanium Alloys under Isothermal and Nonisothermal Hot-Working conditions," *Metallurgical and Materials Transaction*, 33A, (2002), 2719-2727.
- Toubal, L.; Bocher, P.; Moreau, A.: Dwell fatigue life dispersion of a near alpha titanium. Alloy. *International Journal of Fatigue* 31, (2009), 601-605
- Uta, E.: Etude des hétérogénéités de texture et de microstructure au sein de disques forgés en IMI834 : Influence sur les propriétés en fatigue-dwell. Ph.D. thesis, Université de Metz (2009).
- Vo, P.; Jahazi, M.; Yue, S.; Bocher, P.: Modelling flow stress of a near-alpha titanium alloy, *Materials Science and Engineering*. 447, (2007), 99-110.
- Wolfram, S.: Cellular automata as models of complexity. *Nature*, 311, 5985, (1984) 419-424

---

*Addresses:* Redouane Bastajib, Nabil Boutana, Philippe Bocher, École de technologie supérieure, 1100 rue Notre-Dame Ouest, Montréal (QC) Canada H3C 1K3 ; Mohammed Jahazi, Centre des Technologies de Fabrication en Aérospatiale (CTFA), 5145, avenue Decelles, Montréal, Canada H3T 2B2.  
email: Philippe.Bocher@etsmtl.ca; Mohammad.Jahazi@cnrc-nrc.gc.ca.